

Hourglass-Like Spin Excitation in a Doped Mott Insulator

Jia-Xin Zhang,^{1,*} Chuan Chen,^{1,†} Jian-Hao Zhang,² and Zheng-Yu Weng¹

¹*Institute for Advanced Study, Tsinghua University, Beijing 100084, China*

²*Department of Physics, The Pennsylvania State University, University Park, Pennsylvania 16802, USA*

(Dated: July 13, 2023)

We examine the dynamical magnetic response in a two-component resonating-valence-bond (RVB) description of the doped Mott insulator. The half-filled antiferromagnetic phase described by the Schwinger-boson mean-field theory will evolve into a bosonic-RVB state in the superconducting phase upon doping, where the doped holes introduce another fermionic itinerant spinon which forms a BCS-like RVB order. The spin excitations are thus composed of a resonance-like mode from the former and a weak dispersive mode from the itinerant component at the mean-field level. These two-component spinons are shown to give rise to an hourglass-like spin excitation at the RPA level via an antiferromagnetic coupling between the two modes, which provides an unconventional explanation of the experimental observations in the cuprate. In particular, we also discuss an instability towards an incommensurate magnetic order in this theoretical framework.

Introduction.—The spin dynamics is essential for understanding the mechanism of the cuprate superconductor, which reduces to the only relevant low-lying mode in the undoped limit [1]. At finite doping, the dynamic spin susceptibility measured by the inelastic neutron scattering (INS) reveals that the gapless spin-wave [2, 3] at the antiferromagnetic (AFM) wave vector $\mathbf{Q}_0 = (\pi, \pi)$ becomes gapped with the destruction of the AFM long-range order. The spin excitation further displays a resonance-like mode [4–10] with a characteristic energy E_g . Slightly deviating from \mathbf{Q}_0 , the resonance mode splits and extends to both higher and lower energies to result in the well-known hourglass-shaped spectrum [11–19].

Phenomenologically, two distinct starting points have been commonly employed to describe the experimentally observed dynamical spin susceptibility. One is based on the itinerant magnetism approach [20–22], where the spin resonance formation below T_c originates from the enhanced feedback effect of the d -wave superconductivity for quasiparticles with a large Fermi surface. Alternatively, the local moment approach [23–26] starts with the undoped two-dimensional (2D) AFM state by examining a mixture of local spins described by the superexchange interaction J and itinerant carriers with tight-binding energy dispersion.

Microscopically, the parent compound of the cuprate acts as a Mott insulator, in which all the electrons form local magnetic moments as described by the minimal AFM Heisenberg model at half-filling. How such an AFM state can be doped into a short-range AF state at finite doping has been a central issue in the study of the doped Mott insulator, which is described by an effective one-band model, e.g., the t - J model [27, 28]. The fermionic RVB state was originally proposed by Anderson [27, 29] is one of the conjectures for such a phase, which results in a d -wave Superconducting (SC) instability at low temperatures [30, 31]. Nevertheless, this fermionic RVB state seems incompatible with the Schwinger-boson

or bosonic RVB description[1, 32–34] of the AFM state at half-filling, and how to bridge the two phases still remains unclear [1, 35]. Recently, a two-component RVB description has been proposed[36–38], which theorizes doping an AFM state into a short-range AF state with an intrinsic low-temperature SC instability. Here the AFM phase is well characterized by the Schwinger-boson mean-field state at half-filling, which is then turned into a bosonic RVB state by doping due to the phase-string effect[37, 39] generally associated with a doped Mott insulator. The latter will lead to a nontrivial spin-current backflow created by doped holes moving in a spin singlet background[40, 41]. The resulting spin current, in combination with the doped holes, gives rise to distinct spinons which are fermionic and itinerant in nature[37, 38].

In this paper, we study an unconventional spin excitation in the doped Mott insulator at finite doping as the consequence of such a two-component RVB description. At the RPA level, such a new spin excitation is hourglass-like, which is composed of the bosonic spinons evolved from the Schwinger bosons at half-filling and the itinerant fermionic spinons emerging upon doping. The result is consistent with the INS observations[4–10] in the cuprate. Further physical implications are also discussed.

Emergent two-component RVB description at finite doping.— Starting from the half-filling by doping, a two-component RVB description of the short-range AF state has been recently proposed[36, 37] based on the t - J model, whose ground state is given by

$$|\Psi_G\rangle = \hat{\mathcal{P}} \left[e^{i\hat{\Theta}} |\Phi_h\rangle \otimes |\Phi_a\rangle \otimes |\Phi_b\rangle \right]. \quad (1)$$

Here $|\Phi_b\rangle$ originated from the Schwinger-boson mean-field state at half-filling and is known as the bosonic RVB state[shown by blue thick lines in Fig.1(b)], $|\Phi_a\rangle$ is a BCS-like state[shown by blue wave lines in Fig.1(b)] formed by the *fermionic* spinons which are introduced by the doped holes, and $|\Phi_h\rangle$ describes a Bose-condensed state of the bosonic holons which are also introduced by the doped holes as carrying electric charges.

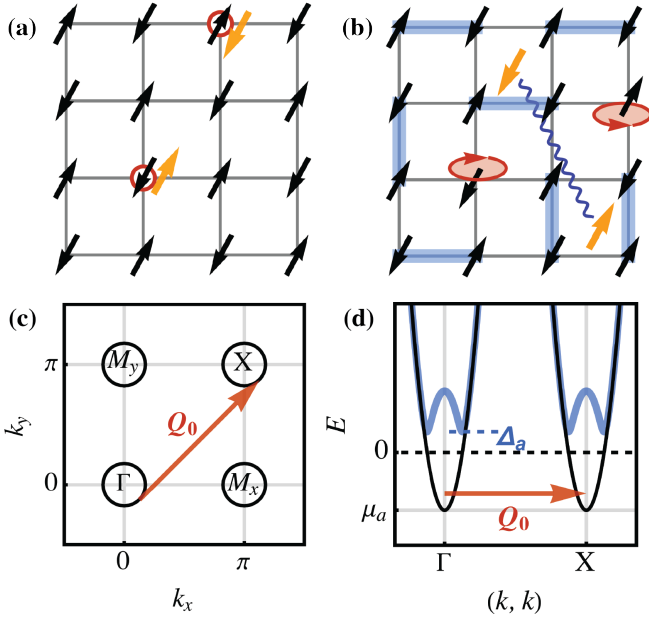


FIG. 1. Schematic illustration of the two-component spinons in a doped Mott insulator. (a) A bare hole is composed of a bosonic holon (red circle) and a fermionic a -spinon (orange arrow) in a spin background filled with the single-occupied bosonic b -spinons (black arrow) such that the total spin at the hole site is zero; (b) Two-component RVB state in which holons are condensed and b -spinons form singlet RVB pairings (blue lines), with each unpaired b -spinon carrying a π -vortex (red circle with arrow) of the charge supercurrent. Concurrently, the a -spinons are in an s -wave pairing (wavy lines); (c) Four Fermi pockets for the a -spinons emerge if the pairing order parameter Δ_a vanishes. The red arrow denotes the AFM wavevector $\mathbf{Q}_0 = (\pi, \pi)$; (d) Energy dispersion of the a -spinon near Γ and X pockets displayed by black curves for $\Delta_a = 0$ and blue curves for $\Delta_a \neq 0$.

The unitary operator $e^{i\hat{\Theta}}$ in Eq. (1) is a duality transformation to implement the so-called phase-string effect[37, 39], which is very singular as created by the doped holes. The projection operator $\hat{\mathcal{P}}$ further enforces the constraint between the three fractionalized sub-systems in Eq. (1) by

$$n_i^h S_b^z(\mathbf{r}_i) = -S_a^z(\mathbf{r}_i), \quad (2)$$

in which n_i^h is the holon number at site i , and S_a^z and S_b^z denote the z -component spins of the a -spinon and b -spinon, respectively. Physically, Eq.(2) means the half-filled b -spinons at the hole sites must be compensated by the a -spinons, whose number is equal to the hole number[depicted in Fig. 1(a)]. Previously, the individual behaviors for $|\Phi_b\rangle$, and $|\Phi_a\rangle$ have been studied[37, 38, 42, 43], whose results will be first given in the following. Then the effect of $\hat{\mathcal{P}}$ in Eq. (2) will be further incorporated at the RPA level.

Local moments.— At half-filling, the ground state of the Heisenberg Hamiltonian is well described by the

Schwinger-boson mean-field state[1, 32–34], which will evolve into the short-range AF state $|\Phi_b\rangle$ at finite doping as outlined above[cf. blue thick line in Fig. 1(b)]. In contrast to conventional Schwinger bosons with continuous spectra [33], the b -spinons in this study exhibit dispersionless, “Landau-level-like” discrete energy levels with a gap E_s [38, 43, 44]. Consequently, the corresponding low-lying dynamical spin susceptibility originating from the lowest Landau level is given by as [38, 42–44]

$$\chi_b(i\nu_n, \mathbf{Q}) = \text{wavy} = a_c^2 D e^{-\frac{a_c^2}{2}(\mathbf{Q}-\mathbf{Q}_0)^2} \quad (3) \\ \times \left(\frac{1}{i\Omega_n - E_g} - \frac{1}{i\Omega_n + E_g} \right),$$

where $E_g = 2E_s$ represents the resonance energy, the “cyclotron length” $a_c = a/\sqrt{\pi\delta}$ determines the effective spin-spin correlation length[a for lattice constant, δ for doped hole density], and the weight D is not sensitive to doping [44]. As depicted in Fig. 2(a), the spin-wave excitation, derived from the imaginary component of Eq. (3), becomes a gapped resonance-like mode near $\mathbf{Q}_0 = (\pi, \pi)$.

Itinerant spinons.— The doped holes are created by removing spins from the half-filling spin-singlet background characterized by $|\Phi_b\rangle$. The doping introduces new spinons centered at the hole sites known as the a -spinons [the yellow arrows in Fig. 1(a)], which form the itinerant RVB state $|\Phi_a\rangle$ in Eq. (1) [cf. blue wave line in Fig. 1(b)].

The a -spinons as fermions form the multi-pocket Fermi surfaces illustrated in Fig. 1(c), which are determined by:

$$H_a = \sum_{\mathbf{K}, \mathbf{k}} \epsilon_{\mathbf{K}}(\mathbf{k}) a_{\mathbf{K}+\mathbf{k}, \sigma}^\dagger a_{\mathbf{K}, \sigma} \\ + \sum_{\mathbf{K}, \mathbf{k}} \Delta_a a_{\mathbf{K}+\mathbf{k}, \uparrow}^\dagger a_{\mathbf{K}-\mathbf{k}, \downarrow}^\dagger + \text{h.c.} \quad (4)$$

Here $a_{\mathbf{K}+\mathbf{k}, \sigma}^\dagger$ denotes the creation operator for an itinerant a -spinons from pockets $\mathbf{K} = \Gamma, X, M$ with relative momentum \mathbf{k} [depicted in Fig. 1(c)], whose band energy reads $\epsilon_{\mathbf{K}}(\mathbf{k}) = \mathbf{k}^2/2m_a - \mu_a$. The Δ_a term characterizes the uniform s -wave pairing within all pockets. We also assume identical parabolic band structures for all pockets as shown in Fig. 1(d), implying a consistent effective mass m_a and chemical potential μ_a . This model aligns with hopping fermions in the π flux states, displaying well-nested, distinct pockets [37, 38, 44, 45]. Importantly, the Luttinger sum rule for itinerant a -spinons, which arise from doped holes, is associated with the doping density δ , represented as $\sum_{\mathbf{k}, \sigma} n_{\mathbf{k}, \sigma}^a / N = \delta$ [where $n_{\mathbf{k}, \sigma}^a$ denotes the a -spinon number operator and N denotes the total number of sites], rather than half-filling as in conventional spin liquids [46]. This relationship determines the chemical potential μ_a .

The dynamical spin susceptibility of itinerant a -spinons is defined as $\chi_a(r_i - r_j) = \langle S_a^z(r_i) S_a^z(r_j) \rangle$, with

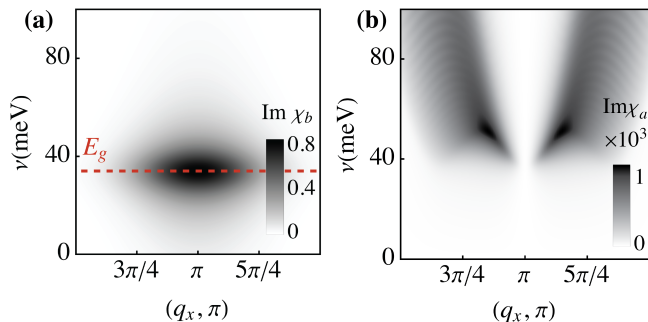


FIG. 2. (a) Imaginary part of bare dynamic spin susceptibility $\text{Im} \chi_b(q)$ for b -spinons, derived from Eq. (3) near the AFM wave vector \mathbf{Q}_0 at $\delta = 0.1$, with the red dashed line indicating the resonance energy E_g . (b) Corresponding susceptibility $\text{Im} \chi_a(q)$ for a -spinons, obtained from Eq. (5). Parameter values are provided in the main text.

$r_i = (\tau_i, \mathbf{r}_i)$ representing the time-space vector. The χ_a can be formulated in the frequency-momentum space as:

$$\chi_a(i\nu_n, \mathbf{q}) = \begin{array}{c} \text{---} \circ \text{---} \\ \text{---} \circ \text{---} \end{array} = -\frac{1}{2N} \sum_{\mathbf{k}} \left(1 - \frac{\Delta_a^2 + \epsilon_{\mathbf{k}+\mathbf{q}} \epsilon_{\mathbf{k}}}{E_{\mathbf{k}+\mathbf{q}} E_{\mathbf{k}}} \right) \times \left(\frac{1}{i\nu_n - E_{\mathbf{k}+\mathbf{q}} - E_{\mathbf{k}}} - \frac{1}{i\nu_n + E_{\mathbf{k}+\mathbf{q}} + E_{\mathbf{k}}} \right), \quad (5)$$

where the term in the first parenthesis represents the coherence factor due to BCS-type pairing and the solid line --- formally denotes the a -spinon propagator. The \mathbf{q} in Eq. (5) denotes the momentum deviation from all the nesting vectors, such as $(0, 0)$, (π, π) , $(0, \pi)$, or $(\pi, 0)$, and it can be easily verified that they are identical.

The dynamic spin susceptibility is given by $\text{Im} \chi(\nu + i0^+, \mathbf{q})$ after the analytic continuation $i\nu_n \rightarrow \nu + i0^+$, as depicted in Fig. 2(b). The spin spectrum around the AFM wave vector \mathbf{Q}_0 , contributed by the scattering between $\Gamma(M_x)$ and $X(M_y)$ pockets, exhibits a continuum above the gap $2\Delta_a$. A significant feature is the complete disappearance of the weight at exact $\mathbf{Q}_0 = (\pi, \pi)$ due to the coherence factor effect [47–50] of the uniform s -wave pairing, i.e., $1 - (\Delta_a^2 + \epsilon_{\mathbf{k}+\mathbf{q}} \epsilon_{\mathbf{k}})/E_{\mathbf{k}+\mathbf{q}} E_{\mathbf{k}} \xrightarrow{\mathbf{q} \rightarrow 0} 0$, which is crucial in yielding an “hourglass” dispersion in the subsequent results.

Hybrid model.— So far at the mean-field level, two-component a and b spinons are separated. At the next step, the local spin constraint Eq. (2) will be incorporated at the RPA level via the following local coupling, which is given by:

$$H_{\text{int}} = g \sum_i S_a^z(\mathbf{r}_i) S_b^z(\mathbf{r}_i), \quad (6)$$

where $g > 0$ represents the strength of this effective interaction. At the RPA level, the dynamical spin susceptibility based on Eq. (6) can be diagrammatically expressed

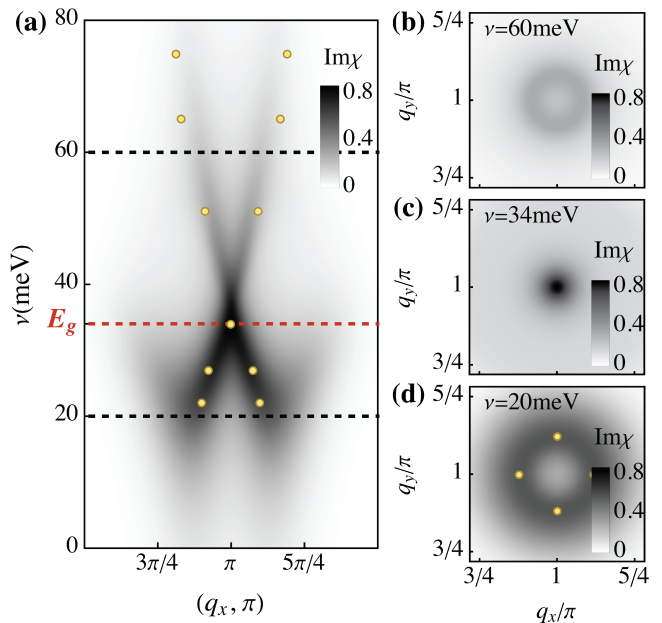


FIG. 3. (a) Imaginary part of dynamic spin susceptibility at RPA level, $\text{Im} \chi^{\text{RPA}}(q)$, determined by Eq. (7) around AFM wave vector \mathbf{Q}_0 at $\delta = 0.1$ and $g = 60 \text{ meV}$. (b)-(d) Calculated slices of $\text{Im} \chi^{\text{RPA}}(q)$ at frequencies indicated by dashed lines in (a). Yellow points in (a) and (d) represent INS results observed in Ref. 17.

as:

$$\chi^{\text{RPA}}(q) = \text{---} + \begin{array}{c} \text{---} \circ \text{---} \\ \text{---} \circ \text{---} \end{array} + \begin{array}{c} \text{---} \circ \text{---} \\ \text{---} \circ \text{---} \end{array} + \dots = \frac{\chi_b(q)}{1 - g^2 \chi_a(q) \chi_b(q)}. \quad (7)$$

The low-energy spin spectrum, $\text{Im} \chi^{\text{RPA}}(q)$, around the AFM wave vector \mathbf{Q}_0 is depicted in Fig. 3(a) at $\delta = 0.1$, resembling the well-known “hourglass” spectrum observed in INS[11–19][with experimental results[17] marked by yellow points in Fig. 3(a)].

In details, the lower branch of the “hourglass” can be interpreted as the resonance modes[shown in Fig. 2(a)] originating from local moments, influenced by itinerant spin modes[displayed in Fig. 2(b)] through the “level repulsion” of RPA correction, resulting in the transfer of spectral weight to lower energy around the \mathbf{Q}_0 . It is essential to emphasize that the resonance mode at the exact \mathbf{Q}_0 -point with characteristic energy E_g remains protected without any spectral weight transfer. This protection results from the complete disappearance of the a -spinon dynamical spin susceptibility χ_a at this momentum due to the coherence factor effects discussed earlier. On the other hand, the spin fluctuation from fermionic itinerant a -spinons near \mathbf{Q}_0 is enhanced with the aid of that from local moments via the term $1 - g^2 \chi_a(q) \chi_b(q)$ in RPA correction Eq. (7), leading to

the upper branch in Fig. 2(b), which is relatively comparable to the lower branch primarily contributed by local moments. Additionally, the frequency slices of the calculated spin fluctuation spectrum for χ^{RPA} around \mathbf{Q}_0 displayed in Fig. 3(b)-(d) exhibit circular features deviating from E_g . This is distinct from the experimentally observed four weight peaks[11–19] marked by yellow points in Fig. 3(d), suggesting that a higher-order correction might be needed to enhance them.

It is worth noting that all phenomenological parameters in our model include the resonance energy E_g , determined directly by the peak of weight in INS[4–10], as well as m_a and Δ_a for fermionic itinerant a -spinons, and the coupling strength g . In this study, at $\delta = 0.1$, we choose $2\Delta_a = 1.1E_g$, $m_a = 1/J$, and $g = 60\text{meV}$ to fit the experimental data, with $J = 120\text{meV}$ representing the bare spin exchange interaction. Also, the doping evolution of m_a can be inferred from the relative change in the residual uniform spin susceptibility at low temperatures under strong magnetic fields[51], the relationship with m_a will be discussed in subsequent sections. Furthermore, we show that the existence of the hourglass structure is insensitive to the specific choice of these parameters[44], as long as the gap $2\Delta_a$ does not differ too much from the resonance energy E_g .

Incommensurate magnetic instability.— When the coupling strength g approaches a critical value g_c , sign changes in static susceptibility become possible, i.e., $\text{Re}\chi^{\text{RPA}}(\omega = 0, \mathbf{Q}_{\text{in}}) < 0$ as illustrated in Fig. 4(b), at incommensurate momenta $\mathbf{Q}_{\text{in}} \equiv \mathbf{Q}_0 + \Delta\mathbf{q}$, alongside the gapless spin excitation shown in Fig. 4(a) stemming from the extension of the lower branch of the “hourglass” structure[with \mathbf{Q}_{in} marked by red arrows in Fig. 4(a)]. This results in the emergence of incommensurate magnetic instability with wave vectors \mathbf{Q}_{in} , which may be associated with stripe order[18, 52–58] once circular gapless modes further break rotational symmetry and select a specific direction due to higher-order corrections.

Furthermore, the determination of the deviating incommensurate wave vector $\Delta\mathbf{q}$ for magnetic instability is related to the pocket size of itinerant a -spinon and the width of resonance modes, both of which increase with the rise in doping density δ . As depicted in Fig. 4(c), the doping evolution of $\Delta\mathbf{q}$ is consistent with experimental and theoretical conclusions[18, 55], i.e., $2\pi\delta$ as indicated by the dashed line.

Uniform susceptibility.— The uniform static susceptibility in our study is contributed by both a -spinons and b -spinons, denoted as $\chi^{\text{loc}} = \chi_b^{\text{loc}} + \chi_a^{\text{loc}}$. Due to the existence of an energy gap for both a -spinons and b -spinons, the uniform static susceptibility χ^{loc} appears to be significantly suppressed at temperatures close to zero. Nonetheless, in a specific situation where a strong magnetic field is applied, it is possible to suppress Δ_a at the conventional vortex cores mediated by the emergent $U(1)$ gauge field between holons and a -spinons from

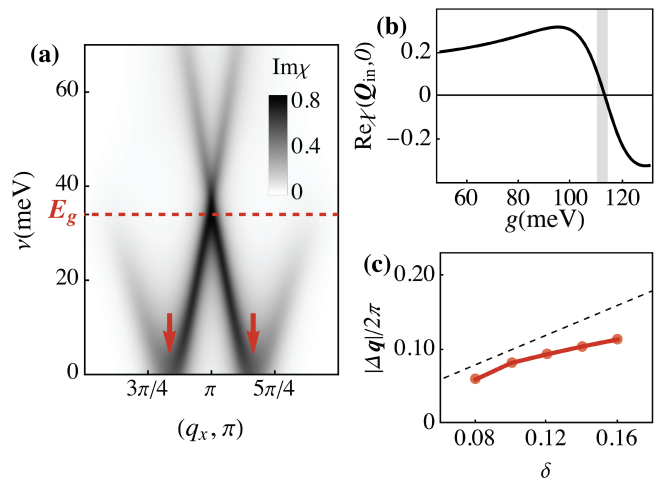


FIG. 4. (a) Calculated $\text{Im}\chi^{\text{RPA}}(g)$ using Eq. (7) at $\delta = 0.1$ and $g = g_c$ displays gapless spin modes with incommensurate wave vector \mathbf{Q}_{in} (red arrows). (b) Static spin susceptibility at \mathbf{Q}_{in} determined by the real part of Eq. (7), showing sign change at $g = g_c$ (gray region). (c) Comparison of calculated doping evolution of $\Delta\mathbf{q}$ with experimental rule $2\pi\delta$ (dashed line).

the constraint Eq. (2)[44]. Consequently, a finite DOS of $\mathcal{N}(0) = \frac{a^2}{2\pi\hbar^2}m_a$ from the gapless Fermi pockets of a -spinon can be restored at these vortex cores, resulting in a finite residual $\chi_a^{\text{loc}} \propto \mathcal{N}(0)$ at low temperatures in cuprates, which is in agreement with the observed NMR results[51, 59]. Further details regarding the temperature evolution of χ^{loc} can be found in Ref. 44.

In addition, our previous work[37, 38] suggests that the emergence of gapless a -spinon Fermi pockets when Δ_a is suppressed by strong magnetic fields can also account for the observed linear- T heat capacity[59–61] and the quantum oscillations[62, 63] associated with pocket physics.

Discussion.—The hourglass-like spin excitation has been discussed as the consequence of a two-component RVB description of the doped Mott insulator at finite doping. Here two-component spinons characterize the local and itinerant spin moments emerging upon doping the single-band t - J model, in contrast to the single-component spinon in the original RVB theory proposed by Anderson[27, 29]. Note that the separation of itinerant spins (electrons) and local moments is a natural concept in multi-band systems such as the heavy fermion systems with Kondo coupling [64–66] and iron-based superconductors with Hund’s rule coupling [67–71], where the mutual interaction between the two degrees of freedom produces the correct low-lying spin excitations. In the present study, the emergence of two distinct spin components is due to the unique strong correlation effect within a single-band system that results in fractionalization. Specifically, the itinerant fermionic a -spinons carry the spin degrees of freedom associated with hop-

ping holes, while the b -spinons describe the background local moments persisting from the half-filling. The interaction between these two components, as described in Eq. (2), arises from the no-double-occupancy constraint in the t - J model.

In our study, the hourglass spectrum uniquely relies on the coherence factor effect [47–50] of the s -wave pairing Δ^a of the itinerant spinons. It is worth pointing out that, within this framework (in the presence of holon condensation), the superconducting order parameters have a composition structure given by $\langle \hat{c}_{i\uparrow} \hat{c}_{j\downarrow} \rangle \propto \Delta_{ij}^a \langle e^{i\frac{1}{2}(\Phi_i^s + \Phi_j^s)} \rangle$, where the amplitude Δ^a is s -wave-like while the d -wave pairing symmetry as well as the phase coherence arise from the phase factor $e^{i\frac{1}{2}(\Phi_i^s + \Phi_j^s)}$ contributed by the b -spinons [37, 38, 45]. Such a hidden s -wave component with a BCS-like d -wave pairing order parameter leads to a novel pairing-symmetry dichotomy, which has been revealed and discussed in recent numerical[41] and may have important experimental implications[72–74]. Here the phase transition near T_c is dictated by the free b -spinon excitations carrying the π -vortices [37, 42, 44]. Finally, we shall show elsewhere how the spin excitations discussed in the present work may also naturally reduce to a commensurate AFM Goldstone mode in a dilute doping limit.

Acknowledgments.— We acknowledge stimulating discussions with Zhi-Jian Song, Zhen Bi, and Ji-Si Xu. J.-X.Z., C.C., and Z.-Y.W. are supported by MOST of China (Grant No. 2017YFA0302902). C.C. acknowledges the support from the Shuimu Tsinghua Scholar Program. J.H.Z. is supported by a startup fund from the Pennsylvania State University (Zhen Bi), and thanks the hospitality of the Kavli Institute for Theoretical Physics, which is partially supported by the National Science Foundation under Grant No. NSF PHY-1748958.

* These authors contributed equally to this work; zjx19@mails.tsinghua.edu.cn

† These authors contributed equally to this work

- [1] P. A. Lee, N. Nagaosa, and X.-G. Wen, *Rev. Mod. Phys.* **78**, 17 (2006).
- [2] R. Coldea, S. M. Hayden, G. Aeppli, T. G. Perring, C. D. Frost, T. E. Mason, S.-W. Cheong, and Z. Fisk, *Phys. Rev. Lett* **86**, 5377 (2001).
- [3] N. S. Headings, S. M. Hayden, R. Coldea, and T. G. Perring, *Phys. Rev. Lett* **105**, 247001 (2010).
- [4] H. F. Fong, B. Keimer, P. W. Anderson, D. Reznik, F. Doğan, and I. A. Aksay, *Phys. Rev. Lett.* **75**, 316 (1995).
- [5] H. He, Y. Sidis, P. Bourges, G. D. Gu, A. Ivanov, N. Koshizuka, B. Liang, C. T. Lin, L. P. Regnault, E. Schoenher, and B. Keimer, *Phys. Rev. Lett.* **86**, 1610 (2001).
- [6] B. Fauque, Y. Sidis, L. Capogna, A. Ivanov, K. Hradil, C. Ulrich, A. I. Rykov, B. Keimer, and P. Bourges, *Phys. Rev. B* **76**, 214512 (2007).
- [7] L. Capogna, B. Fauque, Y. Sidis, C. Ulrich, P. Bourges, S. Pailhes, A. Ivanov, J. L. Tallon, B. Liang, C. T. Lin, A. I. Rykov, and B. Keimer, *Phys. Rev. B* **75**, 060502(R) (2007).
- [8] H. F. Fong, P. Bourges, Y. Sidis, L. P. Regnault, A. Ivanov, G. D. Gu, N. Koshizuka, and B. Keimer, *Nature* **398**, 588 (1999).
- [9] H. He, P. Bourges, Y. Sidis, C. Ulrich, L. P. Regnault, S. Pailhes, N. S. Berzigiarova, N. N. Kolesnikov, and B. Keimer, *Science* **295**, 1045 (2002).
- [10] P. Dai, H. A. Mook, S. M. Hayden, G. Aeppli, T. G. Perring, R. D. Hunt, and F. Dogan, *Science* **284**, 1344 (1999).
- [11] M. K. Chan, C. J. Dorow, L. Mangin-Thro, Y. Tang, Y. Ge, M. J. Veit, G. Yu, X. Zhao, A. D. Christianson, J. T. Park, Y. Sidis, P. Steffens, D. L. Abernathy, P. Bourges, and M. Greven, *Nat. Commun.* **7**, 10819 (2016).
- [12] M. K. Chan, Y. Tang, C. J. Dorow, J. Jeong, L. Mangin-Thro, M. J. Veit, Y. Ge, D. L. Abernathy, Y. Sidis, P. Bourges, and M. Greven, *Phys. Rev. Lett* **117**, 277002 (2016).
- [13] S. Pailhès, Y. Sidis, P. Bourges, V. Hinkov, A. Ivanov, C. Ulrich, L. P. Regnault, and B. Keimer, *Phys. Rev. Lett* **93**, 167001 (2004).
- [14] V. Hinkov, P. Bourges, S. Pailhès, Y. Sidis, A. Ivanov, C. D. Frost, T. G. Perring, C. T. Lin, D. P. Chen, and B. Keimer, *Nat. Phys.* **3**, 780 (2007).
- [15] G. Xu, G. D. Gu, M. Hücker, B. Fauqué, T. G. Perring, L. P. Regnault, and J. M. Tranquada, *Nat. Phys.* **5**, 642 (2009).
- [16] B. Vignolle, S. M. Hayden, D. F. McMorrow, H. M. Rønnow, B. Lake, C. D. Frost, and T. G. Perring, *Nat. Phys.* **3**, 163 (2007).
- [17] S. M. Hayden, H. A. Mook, P. Dai, T. G. Perring, and F. Dogan, *Nature* **429**, 531 (2004).
- [18] J. M. Tranquada, H. Woo, T. G. Perring, H. Goka, G. D. Gu, G. Xu, M. Fujita, and K. Yamada, *Nature* **429**, 534 (2004).
- [19] K. Sato, K. Ikeuchi, R. Kajimoto, S. Wakimoto, M. Arai, and M. Fujita, *J. Phys. Soc. Jpn.* **89**, 114703 (2020).
- [20] F. Onufrieva and P. Pfeuty, *Phys. Rev. B* **65**, 054515 (2002), theory: itinerant.
- [21] I. Eremin, D. K. Morr, A. V. Chubukov, K. H. Bennemann, and M. R. Norman, *Phys. Rev. Lett* **94**, 147001 (2004), theory: itinerant.
- [22] A. Abanov, A. V. Chubukov, M. Eschrig, M. R. Norman, and J. Schmalian, *Phys. Rev. Lett* **89**, 177002 (2002), theory: itinerant.
- [23] A. Sherman and M. Schreiber, *Phys. Rev. B* **68**, 094519 (2003), theory: local.
- [24] M. V. Eremin, I. M. Shigapov, and I. M. Eremin, *Eur. Phys. J. B* **85**, 131 (2012), theory: local.
- [25] A. J. A. James, R. M. Konik, and T. M. Rice, *Phys. Rev. B* **86**, 100508 (2012), theory: local.
- [26] A. I. Milstein and O. P. Sushkov, *Phys. Rev. B* **78**, 014501 (2008), theory: local.
- [27] P. W. Anderson, *Science* **235**, 1196 (1987).
- [28] F. C. Zhang and T. M. Rice, *Phys. Rev. B* **37**, 3759 (1988).
- [29] G. Baskaran, Z. Zou, and P. Anderson, *Solid State Commun.* **63**, 973 (1987).
- [30] F. C. Zhang, C. Gros, T. M. Rice, and H. Shiba, *Super-*

- cond. Sci. Technol. **1**, 36 (1988).
- [31] G. Kotliar and J. Liu, *Phys. Rev. B* **38**, 5142 (1988).
- [32] B. Chakraborty, N. Read, C. Kane, and P. A. Lee, *Phys. Rev. B* **42**, 4819 (1990).
- [33] D. P. Arovas and A. Auerbach, *Phys. Rev. B* **38**, 316 (1988).
- [34] N. Read and S. Sachdev, *Phys. Rev. Lett.* **66**, 1773 (1991).
- [35] P. A. Lee and N. Nagaosa, *Phys. Rev. B* **46**, 5621 (1992).
- [36] Z.-Y. Weng, *New J. Phys.* **13**, 103039 (2011).
- [37] Y. Ma, P. Ye, and Z.-Y. Weng, *New J. Phys.* **16**, 083039 (2014).
- [38] J.-X. Zhang and Z.-Y. Weng, (2022), arXiv:2208.10519.
- [39] D. N. Sheng, Y. C. Chen, and Z. Y. Weng, *Phys. Rev. Lett.* **77**, 5102 (1996).
- [40] W. Zheng, Z. Zhu, D. N. Sheng, and Z.-Y. Weng, *Phys. Rev. B* **98**, 1 (2018).
- [41] J.-Y. Zhao, S. A. Chen, H.-K. Zhang, and Z.-Y. Weng, *Phys. Rev. X* **12**, 011062 (2022).
- [42] J. W. Mei and Z. Y. Weng, *Phys. Rev. B* **81**, 014507 (2010).
- [43] W. Q. Chen and Z. Y. Weng, *Phys. Rev. B* **71**, 134516 (2005).
- [44] See Supplemental Material for further details.
- [45] J.-H. Zhang, S. Li, Y. Ma, Y. Zhong, H. Ding, and Z.-Y. Weng, *Phys. Rev. Res.* **2**, 023398 (2020).
- [46] Y. Zhou, K. Kanoda, and T.-K. Ng, *Rev. Mod. Phys.* **89**, 025003 (2017).
- [47] H. F. Fong, B. Keimer, P. W. Anderson, D. Reznik, F. Doğan, and I. A. Aksay, *Phys. Rev. Lett* **75**, 316 (1995).
- [48] K. Seo, C. Fang, B. A. Bernevig, and J. Hu, *Phys. Rev. B* **79**, 235207 (2009).
- [49] M. M. Korshunov and I. Eremin, *Phys. Rev. B* **78**, 140509 (2008).
- [50] T. A. Maier and D. J. Scalapino, *Phys. Rev. B* **78**, 020514 (2008).
- [51] S. Kawasaki, C. Lin, P. L. Kuhns, A. P. Reyes, and G.-q. Zheng, *Phys. Rev. Lett* **105**, 137002 (2010).
- [52] J. M. Tranquada, B. J. Sternlieb, J. D. Axe, Y. Nakamura, and S. Uchida, *Nature* **375**, 561 (1995).
- [53] M. Fujita, H. Goka, K. Yamada, and M. Matsuda, *Phys. Rev. Lett* **88**, 167008 (2002).
- [54] J. Zaanen and O. Gunnarsson, *Phys. Rev. B* **40**, 7391 (1989).
- [55] S. A. Kivelson, I. P. Bindloss, E. Fradkin, V. Oganesyan, J. M. Tranquada, A. Kapitulnik, and C. Howald, *Rev. Mod. Phys.* **75**, 1201 (2003).
- [56] B.-X. Zheng, C.-M. Chung, P. Corboz, G. Ehlers, M.-P. Qin, R. M. Noack, H. Shi, S. R. White, S. Zhang, and G. K.-L. Chan, *Science* **358**, 1155 (2017).
- [57] E. W. Huang, C. B. Mendl, S. Liu, S. Johnston, H.-C. Jiang, B. Moritz, and T. P. Devereaux, *Science* **358**, 1161 (2017).
- [58] E. Fradkin, S. A. Kivelson, and J. M. Tranquada, *Rev. Mod. Phys.* **87**, 457 (2015).
- [59] J.-W. Mei, S. Kawasaki, G.-Q. Zheng, Z.-Y. Weng, and X.-G. Wen, *Phys. Rev. B* **85**, 134519 (2012).
- [60] C. Girod, A. Legros, A. Forget, D. Colson, C. Marcenat, A. Demuer, D. LeBoeuf, L. Taillefer, and T. Klein, *Phys. Rev. B* **102**, 014506 (2020).
- [61] H.-H. Wen, G. Mu, H. Luo, H. Yang, L. Shan, C. Ren, P. Cheng, J. Yan, and L. Fang, *Phys. Rev. Lett* **103**, 067002 (2009).
- [62] N. Doiron-Leyraud, C. Proust, D. LeBoeuf, J. Levallois, J.-B. Bonnemaison, R. Liang, D. A. Bonn, W. N. Hardy, and L. Taillefer, *Nature* **447**, 565 (2007).
- [63] N. Barišić, S. Badoux, M. K. Chan, C. Dorow, W. Tabis, B. Vignolle, G. Yu, J. Béard, X. Zhao, C. Proust, and M. Greven, *Nat. Phys.* **9**, 761 (2013).
- [64] A. Auerbach and K. Levin, *Phys. Rev. Lett.* **57**, 877 (1986).
- [65] P. Coleman, *Phys. Rev. B* **29**, 3035 (1984).
- [66] S. Nakatsuji, D. Pines, and Z. Fisk, *Phys. Rev. Lett* **92**, 016401 (2004).
- [67] S.-P. Kou, T. Li, and Z.-Y. Weng, *Europhys Lett.* **88**, 17010 (2009).
- [68] W.-G. Yin, C.-C. Lee, and W. Ku, *Phys. Rev. Lett* **105**, 107004 (2010).
- [69] W. Lv, F. Krüger, and P. Phillips, *Phys. Rev. B* **82**, 045125 (2010).
- [70] L. P. Gor'kov and G. B. Teitel'baum, *Phys. Rev. B* **87**, 024504 (2013).
- [71] Y.-Z. You, F. Yang, S.-P. Kou, and Z.-Y. Weng, *Phys. Rev. B* **84**, 054527 (2011).
- [72] Y. Zhong, Y. Wang, S. Han, Y.-F. Lv, W.-L. Wang, D. Zhang, H. Ding, Y.-M. Zhang, L. Wang, K. He, R. Zhong, J. A. Schneeloch, G.-D. Gu, C.-L. Song, X.-C. Ma, and Q.-K. Xue, *Sci. Bull.* **61**, 1239 (2016).
- [73] M.-Q. Ren, Y.-J. Yan, T. Zhang, and D.-L. Feng, *Chin. Phys. Lett.* **33**, 127402 (2016).
- [74] Y. Zhu, M. Liao, Q. Zhang, H.-Y. Xie, F. Meng, Y. Liu, Z. Bai, S. Ji, J. Zhang, K. Jiang, R. Zhong, J. Schneeloch, G. Gu, L. Gu, X. Ma, D. Zhang, and Q.-K. Xue, *Phys. Rev. X* **11**, 031011 (2021).
- [75] E. I. Rashba, L. E. Zhukov, and A. L. Efros, *Phys. Rev. B* **55**, 5306 (1997).

Supplementary Materials for: “Hourglass-Like Spin Excitation in a Doped Mott Insulator”

In the following supplementary materials, we provide more analytical results to support the conclusions presented in the main text. In Sec. I., we present a detailed derivation of the dynamical spin susceptibility for itinerant fermionic a -spinons, $\chi_a(q)$, as given in Eq. (5). In Sec. II., we give the discrete energy levels for bosonic b -spinons, as well as a comprehensive derivation of the corresponding dynamical spin susceptibility $\chi_b(q)$ in Eq. (3). In Sec. III., we show that the four well-nested Fermi pockets of itinerant a -spinons, discussed in the main text, are consistent with the hopping fermions in the square lattice with uniform π -flux. In Sec. IV., we reveal the existence of two types of vortex excitations in different temperature regions and provide the temperature evolution of spin susceptibility related to vortex states. In Sec. V., we display the dynamical spin susceptibility $\chi^{\text{RPA}}(q)$ at the RPA level with various chosen parameters, illustrating that the “hourglass” feature is not sensitive to the specific parameters.

I. Derivation of Dynamical Spin Susceptibility for Itinerant Fermionic a -Spinons in Eq. (5)

Following the order of particle-hole and pocket degrees of freedom, we arrange the a -spinon operators as:

$$\psi_k = \begin{pmatrix} a_{k\uparrow} \\ a_{-k\downarrow}^\dagger \end{pmatrix} \otimes \begin{pmatrix} \Gamma \\ X \end{pmatrix} \quad (\text{S1})$$

$$\Psi_k = \begin{pmatrix} a_{k\uparrow} \\ a_{-k\downarrow}^\dagger \end{pmatrix} \otimes \begin{pmatrix} M_x \\ M_y \end{pmatrix}, \quad (\text{S2})$$

where $k = (i\omega_n, \mathbf{k})$ refers to the fermionic momentum-frequency vector. This work is primarily focused on the magnetic fluctuation around $\mathbf{Q}_0 = (\pi, \pi)$, thus only the particle-hole scattering between two pockets shifted by \mathbf{Q}_0 is relevant. Specifically, scattering between Γ and X pockets, or M_x and M_y pockets, is considered. Consequently, the pocket indices consist of either (Γ, X) or (M_x, M_y) combinations. Using such representation, the Hamiltonian in Eq. (4) can be written as

$$H_a = \sum_{\mathbf{k}} \psi_{\mathbf{k}}^\dagger h_{\mathbf{k}} \psi_{\mathbf{k}} + \sum_{\mathbf{k}} \Psi_{\mathbf{k}}^\dagger h_{\mathbf{k}} \Psi_{\mathbf{k}} \quad (\text{S3})$$

with

$$h_{\mathbf{k}} = \epsilon_{\mathbf{k}} \sigma_z \otimes \tau_0 + \Delta_a \sigma_x \otimes \tau_0, \quad (\text{S4})$$

where $\epsilon_K(\mathbf{k}) = \mathbf{k}^2/2m_a - \mu_a$ is the dispersion for a -spinons, and σ and τ are Pauli matrices denoting the particle-hole and pocket degrees of freedom, respectively. Therefore, the Green’s function for a -spinon $G_a(k) = -\langle \psi_k \psi_k^\dagger \rangle = -\langle \Psi_k \Psi_k^\dagger \rangle$ is given by:

$$G_a(k) \equiv \text{---} \rightarrow = (i\omega_n \sigma_0 \otimes \tau_0 - h_{\mathbf{k}})^{-1} \quad (\text{S5})$$

$$= \frac{i\omega_n \sigma_0 \otimes \tau_0 + \Delta_a \sigma_x \otimes \tau_0 + \epsilon_{\mathbf{k}} \sigma_z \otimes \tau_0}{(i\omega_n)^2 - E_{\mathbf{k}}^2}, \quad (\text{S6})$$

where $E_{\mathbf{k}} = \sqrt{\epsilon_{\mathbf{k}}^2 + \Delta_a^2}$ is the dispersion for a -spinon with BCS pairing. The dynamical spin susceptibility from itinerant a -spinons is defined as $\chi_a(r_i - r_j) = \langle S_a^z(r_i) S_a^z(r_j) \rangle$. χ_a can be expressed in the frequency-momentum space as follows:

$$\chi_a(q) = -2 \times \frac{1}{4N} \sum_{\mathbf{k}} \text{Tr} G_a(k+q) s_a G_a(k) s_a = \text{---} \circlearrowleft \text{---} \quad (\text{S7})$$

where $s_a = \sigma_0 \otimes \tau_x$ and $s_a = \sigma_0 \otimes \tau_0$ denote the magnetic fluctuation near (π, π) and $(0, 0)$, respectively. Note that the factor 2 in Eq. (S7) arises from the summation over ψ and Ψ components. Following the Matsubara summation, the expression for the dynamical spin susceptibility becomes Eq. (5), which reads:

$$\chi_a(iv_n, \mathbf{q}) = -\frac{1}{2N} \sum_{\mathbf{k}} \left(1 - \frac{\Delta_a^2 + \epsilon_{\mathbf{k}+\mathbf{q}} \epsilon_{\mathbf{k}}}{E_{\mathbf{k}+\mathbf{q}} E_{\mathbf{k}}} \right) \times \left(\frac{1}{iv_n - E_{\mathbf{k}+\mathbf{q}} - E_{\mathbf{k}}} - \frac{1}{iv_n + E_{\mathbf{k}+\mathbf{q}} + E_{\mathbf{k}}} \right), \quad (\text{S8})$$

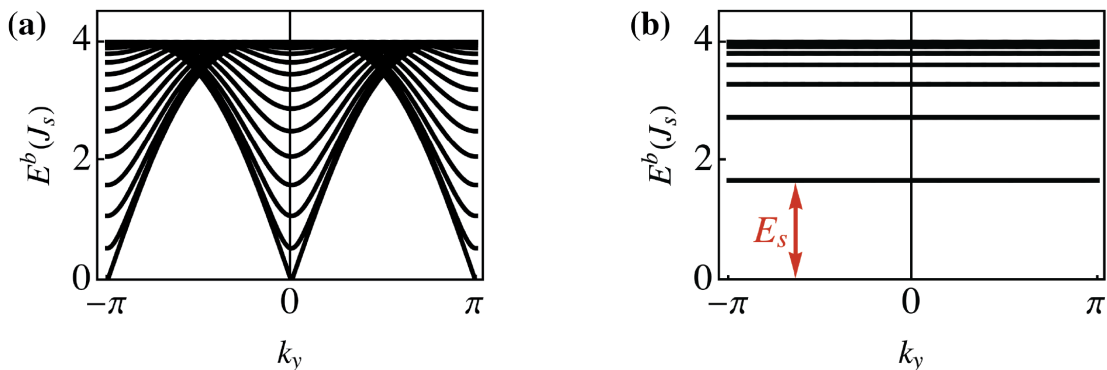


FIG. S1. The dispersion of b -spinons E_m from Eq. (S13) with all quantum numbers plotted along k_y for (a) zero flux and (b) uniform $\delta\pi$ flux in minimum square plateaus. Red arrow indicates lowest excitation level E_s . Parameters: $\delta = 1/8$ and $\lambda_b = 4J_s$.

where \mathbf{q} represents the momentum deviation from $(0,0)$ and (π,π) . Furthermore, by replacing pocket indexes in Eq. (S1) to $(\Gamma M_y)^T$ and $(\Gamma M_x)^T$, the dynamical spin susceptibility χ_a around $(\pi,0)$ and $(0,\pi)$ can be determined, respectively. χ_a is found to be identical across all scenarios where \mathbf{q} deviates from $(0,0)$, $(0,\pi)$, $(\pi,0)$, or (π,π) .

II. Derivation of Dynamical Spin Susceptibility for Background Bosonic b -Spinons in Eq. (3)

The b -spinons in the main text are in the RVB states on a square lattice under uniform magnetic flux. The corresponding Hamiltonian can be expressed as:

$$H_b = -J_s \sum_{\langle ij \rangle, \sigma} b_{i\sigma}^\dagger b_{j-\sigma}^\dagger e^{i\sigma A_{ij}^h} + h.c. + \lambda_b \sum_{i,\sigma} (b_{i\sigma}^\dagger b_{i\sigma} - N), \quad (\text{S9})$$

Here the assumed gauge field A_{ij}^h comes from the mutual Chern-Simons interaction between holons and background b -spinons. Therefore, with the holons condensed, the RVB-pairing b -spinons experience a uniform static gauge field with a $\delta\pi$ flux per plaquette.

Now, the pairing component can be redefined as:

$$\sum_{i,j} b_{i,\uparrow}^\dagger M_{i,j} b_{j,\downarrow}^\dagger + b_{i,\downarrow} M_{i,j} b_{j,\uparrow}, \quad (\text{S10})$$

where M is a hermitian matrix defined as:

$$M_{i,j} = \begin{cases} -J_s e^{iA_{ij}^h} & j \in \text{NN}(i) \\ 0 & \text{others} \end{cases} \quad (\text{S11})$$

Then, with the standard diagonalization procedure as in Hofstadter system, we obtain:

$$H_b = \sum_{m,\sigma} E_m^b \gamma_{m\sigma}^\dagger \gamma_{m\sigma} \quad (\text{S12})$$

with the b -spinons spectrum:

$$E_m^b = \sqrt{\lambda_b^2 - (\xi_m^b)^2} \quad (\text{S13})$$

via introducing the following Bogoliubov transformation:

$$b_{i\sigma} = \sum_m \omega_{m\sigma}(\mathbf{r}_i) \left(u_m \gamma_{m\sigma} - v_m \gamma_{m-\sigma}^\dagger \right), \quad (\text{S14})$$

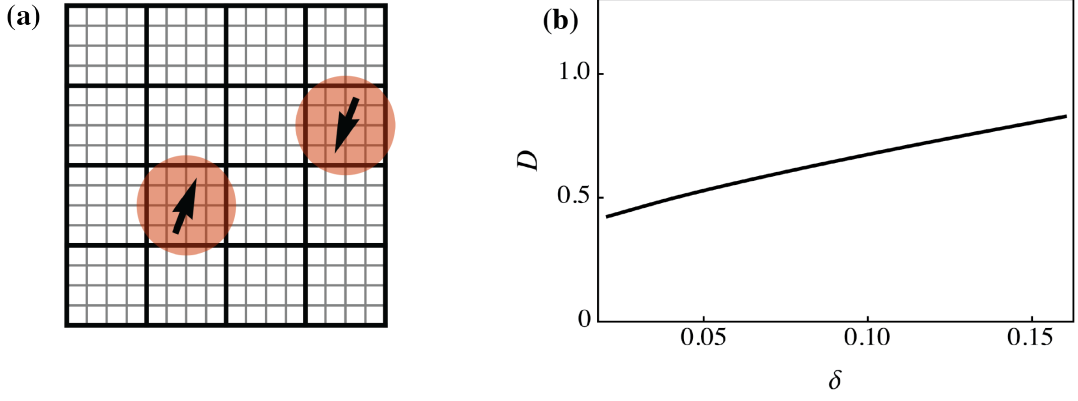


FIG. S2. (a) Depicts b -spinon wave packets, labeled by red disks, with either $w_{m^*}(\mathbf{r})$ or $w_m(\mathbf{r})$ magnetic Wannier wave functions in a square lattice (gray grids). These are positioned within individual magnetic unit cells (black grids). (b) The doping evolution of D in Eq. (S25) as calculated in prior mean-field self-consistent studies[37, 38].

where the coherent factors are given by

$$\begin{aligned}
 u_m &= \sqrt{\frac{1}{2} \left(1 + \frac{\lambda}{E_m^b} \right)} \\
 v_m &= \text{sgn}(\xi_m^b) \sqrt{\frac{1}{2} \left(-1 + \frac{\lambda}{E_m^b} \right)}.
 \end{aligned} \tag{S15}$$

Here, ξ_m^b as well as $w_m(\mathbf{r}_i) \equiv w_{m\sigma}(\mathbf{r}_i) = w_{m-\sigma}^*(\mathbf{r}_i)$ in Eq. (S14) are the eigenfunctions and eigenvalues of the following equation:

$$\xi_m^b \omega_m(\mathbf{r}_i) = -\frac{J\Delta^s}{2} \sum_{j=\text{NN}(i)} e^{i\sigma A_{ij}^h} \omega_m(\mathbf{r}_j). \tag{S16}$$

We select the Landau gauge along the x -axis, as expressed in $A_{i,i+\hat{e}_y}^h = -\delta\pi i_x$. The resulting b -spinon dispersion E_m^b in Eq. (S13) with the unit of J_s is depicted in Fig. S1(b), which manifests the dispersionless, ‘‘Landau-level-like’’ discrete energy levels[38, 43] with a gap E_s [labeled by the red arrow]. For comparison, Fig. S1(a) displays the continuous spectra for conventional Schwinger bosons under zero flux conditions, highlighting the low-lying propagating modes. For the sake of clear representation, we depict all quantum numbers excluding k_y simultaneously in the figures.

Subsequently, using the relation $S_i^{b,z} = \frac{1}{2} \sum_{\sigma} \sigma b_{i\sigma}^{\dagger} b_{i\sigma}$, the Matsubara spin-spin correlation function can be expressed as:

$$\chi_b(\tau, \mathbf{r}_i - \mathbf{r}_j) = \left\langle \hat{T} S_j^{b,z}(\tau) S_i^{b,z}(0) \right\rangle_0 \tag{S17}$$

$$= \frac{1}{4} \sum_{\sigma\sigma'} \sigma\sigma' \left\langle \hat{T} b_{j\sigma}^{\dagger}(\tau) b_{j\sigma}(\tau) b_{i\sigma'}^{\dagger}(0) b_{i\sigma'}(0) \right\rangle_0 \tag{S18}$$

$$= \frac{1}{4} \sum_{\sigma\sigma'} \sigma\sigma' \left[\left\langle \hat{T} b_{j\sigma}^{\dagger}(\tau) b_{i\sigma'}^{\dagger}(0) \right\rangle_0 \left\langle \hat{T} b_{j\sigma}(\tau) b_{i\sigma'}(0) \right\rangle_0 + \left\langle \hat{T} b_{j\sigma}^{\dagger}(\tau) b_{i\sigma'}(0) \right\rangle_0 \left\langle \hat{T} b_{j\sigma}(\tau) b_{i\sigma'}^{\dagger}(0) \right\rangle_0 \right] \tag{S19}$$

where $\langle \rangle_0$ denotes the expectation value under the mean-field state, and the Wick’s theorem is applied in the last line. Then, by using the Bogoliubov transformation Eq. (S14), together with the Green’s function

$$\begin{aligned}
 G_{\gamma}(m, i\omega_n; \sigma) &\equiv -\langle \gamma_{m\sigma}(i\omega_n) \gamma_{m\sigma}^{\dagger}(i\omega_n) \rangle_0 \\
 &= \frac{1}{i\omega_n - E_m^b}
 \end{aligned} \tag{S20}$$

After performing the summation over σ and replacing $w_{m,\sigma}$ with w_m , the Matsubara spin correlation function in

Eq. (S17) at $T = 0$ can be further simplified as:

$$\begin{aligned} \chi_b(i\nu_n, \mathbf{r}_i - \mathbf{r}_j) &= -\frac{1}{4} \sum_{m,n} w_m^*(\mathbf{r}_i) w_m(\mathbf{r}_j) w_n^*(\mathbf{r}_j) w_n(\mathbf{r}_i) (u_m^2 v_n^2 + v_m^2 u_n^2 - 2u_m v_m u_n v_n) \\ &\quad \times \left(\frac{1}{i\nu_n - E_m - E_n} - \frac{1}{i\nu_n + E_m + E_n} \right) \end{aligned} \quad (\text{S21})$$

From the second line of Eq. (S21), the dominant contribution to χ_b evidently originates from the lowest Landau level (LLL), wherein $E_m = E_n = E_s$, leading to $u_m = u_n$ according to Eq. (S15). Thus, the only non-vanishing contributions are from the cases where $v_n = -v_m$, i.e., $\xi_n^b = -\xi_m^b$. Moreover, according to previous works [42, 75], in the LLL, there exists N_m eigenvectors of M matrix in Eq. (S11) (N_m is the number of magnetic unit cells), with $w_m(\mathbf{r})$ peaking at the center of a magnetic unit cell located at \mathbf{R}_m . We term these localized w_m 's as *local* modes (LM). Moreover, for each local mode $w_m(\mathbf{r})$, a corresponding eigenvector $w_{m^*}(\mathbf{r}) = (-1)^{\mathbf{r}} w_m(\mathbf{r})$ exists, and $\xi_{m^*}^b = -\xi_m^b$, therefore $u_{m^*} = u_m$ and $v_{m^*} = -v_m$. We term these w_{m^*} 's as π -shifted modes.

The Bogoliubov quasiparticles corresponding to both local and π -shifted modes possess a common energy E_s and a common u_m , but v_m differs in sign between these two classes of modes. In essence, under this approximation, the low-lying spin spectrum χ_b will be dominated by the localized b -spinon excitations, which are non-propagating modes with an intrinsic size on the order of a ‘‘cyclotron length’’, a_c . These spinon wave packets with magnetic Wannier wave functions $w_{m^*}(\mathbf{r})$ or $w_m(\mathbf{r})$ are situated in separate magnetic unit cells and are highly degenerate, as illustrated in Fig. S2(a).

In the summation of Eq. (S21), m and n will be either local or π -shifted modes, thus we find:

$$\begin{aligned} \chi_b(i\nu_n, \mathbf{r}_i - \mathbf{r}_j) &= \frac{1}{4} (-1)^{\mathbf{r}_i - \mathbf{r}_j} 2 \left| \sum_{m \in \text{LM}} w_m^*(\mathbf{r}_i) w_m(\mathbf{r}_j) \right|^2 \left(1 - \frac{4\lambda_b^2}{E_g^2} \right) \left(\frac{1}{i\nu_n - E_g} - \frac{1}{i\nu_n + E_g} \right) \\ &= \frac{1}{4} (-1)^{\mathbf{r}_i - \mathbf{r}_j} e^{-\frac{1}{2a_c^2}(\mathbf{r}_i - \mathbf{r}_j)^2} \frac{1}{2\pi^2 a_c^4} \left(1 - \frac{4\lambda_b^2}{E_g^2} \right) \left(\frac{1}{i\nu_n - E_g} - \frac{1}{i\nu_n + E_g} \right). \end{aligned} \quad (\text{S22})$$

where $E_g = 2E_s$ is the resonance energy discussed in the main text. Here, we employ the fact that:

$$\left| \sum_{m \in \text{LM}} w_m^*(\mathbf{r}) w_m(\mathbf{r}') \right| = \frac{1}{2\pi a_c^2} e^{-(\mathbf{r} - \mathbf{r}')^2 / 4a_c^2}, \quad (\text{S23})$$

where $a_c = 1/\sqrt{\pi\delta}$ is the cyclotron length, and we assume lattice constants to be unit, i.e., $a = 1$ for simplicity. By executing a Fourier transformation into the momentum space, we can obtain the expression in Eq. (3):

$$\begin{aligned} \chi_b(i\nu_n, \mathbf{Q}) &= \text{wavy} = \frac{1}{N} \sum_{\mathbf{r}} \chi_b(i\nu_n, \mathbf{r}) e^{-i\mathbf{Q} \cdot \mathbf{r}} \\ &= \frac{1}{4} \frac{1}{\pi a_c^2} \left(1 - \frac{4\lambda_b^2}{E_g^2} \right) e^{-\frac{a_c^2}{2}(\mathbf{Q} - \mathbf{Q}_0)^2} \left(\frac{1}{i\nu_n - E_g} - \frac{1}{i\nu_n + E_g} \right) \\ &= a_c^2 D e^{-\frac{a_c^2}{2}(\mathbf{Q} - \mathbf{Q}_0)^2} \times \left(\frac{1}{i\nu_n - E_g} - \frac{1}{i\nu_n + E_g} \right), \end{aligned} \quad (\text{S24})$$

where $\mathbf{Q}_0 = (\pi, \pi)$ is the AFM wave vector, and D is defined as:

$$D \equiv \frac{1}{4} \frac{1}{\pi a_c^4} \left(1 - \frac{4\lambda_b^2}{E_g^2} \right). \quad (\text{S25})$$

The doping dependence of the weight of χ_b is mainly contributed from a_c^2 in the last line of Eq. (S24), rather than from the value of D . Fig. S2(b) shows the doping evolution of D based on the mean-field self-consistent calculation from the prior work [37, 38], demonstrating the insensitivity of D with respect to the doping density δ .

III. BCS States of Fermions in a Square Lattice with Uniform π -Flux

Assume that fermions form nearest-neighbor (NN) pairing on a square lattice with uniform π flux, as depicted in Fig. S3(a). The Hamiltonian for this setup is provided in

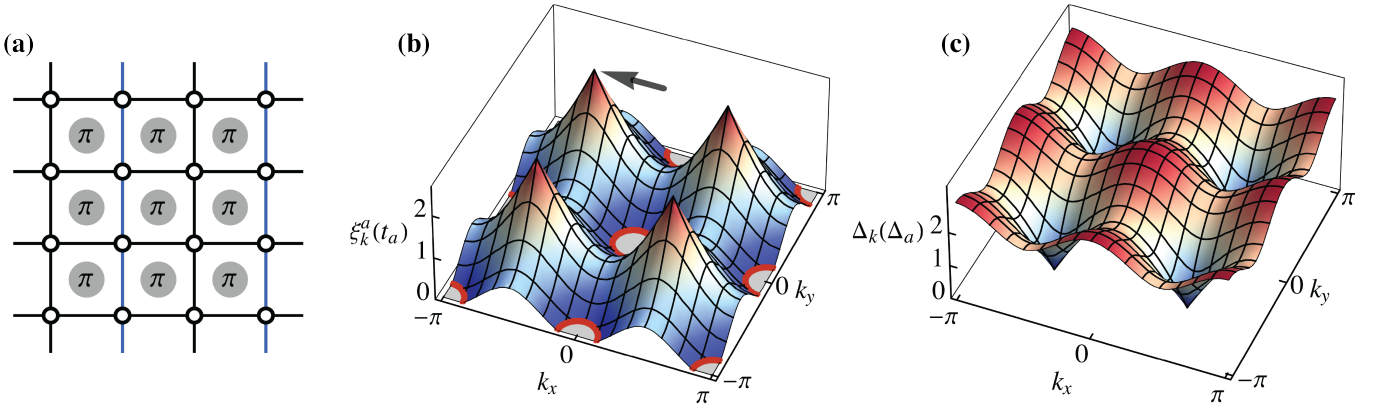


FIG. S3. (a) Square lattice illustration with uniform π -flux. One possible gauge choice for ϕ_{ij}^0 is shown, with black bonds for nearest-neighbor links ($e^{i\phi_{ij}^0} = +1$) and blue bonds for links with $e^{i\phi_{ij}^0} = -1$. (b) The dispersion $\xi_{k,-}$ (from Eq. (S28)) of free fermions in a square lattice with uniform π -flux. The red arrow indicates the well-known Dirac point for half-filling ($n = 1$). Red circles denote Fermi pockets at particle density $n = \delta$ ($\delta = 0.1$). (c) Pairing order Δ_k from Eq. (S29).

$$H_\pi = -t_a \sum_{\langle ij \rangle, \sigma} a_{i\sigma}^\dagger a_{j\sigma} e^{-i\phi_{ij}^0} - \Delta_a \sum_{\langle ij \rangle, \sigma} \sigma a_{i\sigma} a_{j\bar{\sigma}} e^{i\phi_{ij}^0} + \text{h.c.} + \lambda_a \left(\sum_{i,\sigma} a_{i\sigma}^\dagger a_{i\sigma} - \delta N \right), \quad (\text{S26})$$

where ϕ_{ij}^0 is the π -flux gauge field, while Δ_a and λ_a denote the NN pairing amplitude and the chemical potential, respectively. The latter constrains the number of fermions to equal that of doping holes. Selecting the Landau gauge displayed in Fig. S3(a) yields the dispersion of Eq. (S26) as presented in

$$E_{k,\pm} = \sqrt{(\xi_{k,\pm})^2 + \Delta_k^2}, \quad (\text{S27})$$

where $\xi_{k,\pm}$ and Δ_k is the dispersion for free fermions and the s -wave BCS type pairing order parameter, as specified in

$$\xi_{k,\pm} = \pm 2t_a \sqrt{\cos^2 k_x + \cos^2 k_y} + \mu_a \quad (\text{S28})$$

$$\Delta_k = 2\Delta_a \sqrt{\cos^2 k_x + \cos^2 k_y}. \quad (\text{S29})$$

The lower branch dispersion $\xi_{k,-}$ from Eq. (S28) is portrayed in Fig. S3(a), exhibiting well-nested Fermi pockets denoted by red circles. Here, we can understand the origin of this gapless “Fermi pockets” as follows: according to the Eq. (S26), in the absence of pairings, free fermions are in the π -flux lattices, of which the half-filled case corresponds to the well-known π -flux state in fermionic spin liquids, with the Fermi surface shrinking to the Dirac point marked by the red arrow in Fig. S3(a). However, the number of fermions corresponds to the doping density δ , not half-filling, which results in the Dirac point transforming into a gapless Fermi pocket, as illustrated by the red circles in Fig. S3(a).

Furthermore, the calculated BCS type pairing order parameter Δ^k is shown in Fig. S3(b), demonstrating a strongly momentum-dependent s -wave without sign flip. As our focus lies on the physics near the Fermi surface of $\xi_{k,-}$ —namely, around $(0, 0)$, $(\pi, 0)$, $(0, \pi)$, and (π, π) —the anisotropy of the pairing amplitude is not crucial.

Finally, the next-nearest neighbor (NNN) hopping term solely opens the gap of Dirac points, as indicated by the red arrows in Fig. S3(a), implying that such further neighbor term would not affect the Fermi pockets, which are our primary concern at low energy. As a result, coupled with the features of well-nested pockets and the s -wave pairing presented in Eq. (S26), hopping fermions on the square lattice with uniform π -flux emerge as a potential model. This model could account for the low-lying physical behaviors of a -spinons discussed in the main text. Moreover, the mean-field phase string theory in earlier work[37, 38] can provide the effective Hamiltonian Eq. (S26).

IV. Vortex Types and Temperature Evolution of Uniform Spin Susceptibility

In phase string theory, we identify two distinct types of "vortices" generated by the magnetic fields. Specifically, under holon condensation, the experimentally observed superconducting order parameters are given by:

$$\langle \hat{c}_{i\uparrow} \hat{c}_{j\downarrow} \rangle \propto \Delta_{ij}^a e^{i\frac{1}{2}(\Phi_i^s + \Phi_j^s)}, \quad (\text{S30})$$

with the d -wave pairing symmetry arising from the phase $e^{i\frac{1}{2}(\Phi_i^s + \Phi_j^s)}$, which is contributed by b -spinons[37, 38, 45]. The magnetic field induces a novel magnetic π -vortex core which entraps a free b -spinon, and suppresses RVB pairing Δ_s , while Δ_a remains unaffected [illustrated in Figure 1(b)]. This gives rise to a phase transition near T_c , manifesting Kosterlitz-Thouless-like behavior[37, 42]. This behavior disrupts only the phase $e^{i\frac{1}{2}(\Phi_i^s + \Phi_j^s)}$ in Eq. (S30) due to the novel magnetic π -vortices.

On the other hand, there also exists the conventional magnetic vortex with a quantization of 2π . This causes the phase of Δ_a in Eq. (S30) to twist, resulting in the unpairing of a -spinons at the vortex cores mediated by the emergent $U(1)$ gauge field, which comes from the constraint Eq. (2). In contrast, b -spinons remain gapped[illustrated in Fig. S4(b)].

The two vortex types appear within distinct temperature domains. At temperatures much lower than E_g/k_B , novel magnetic π -vortices may be energetically unfavorable due to the minimum b -spinon gap $E_s = E_g/2$ required to break an RVB pair. This is in contrast to a conventional 2π -vortex where $\Delta_a = 0$. However, near T_c , π -vortices carrying b -spinons are more readily formed under external magnetic fields, preceding the disruption of superconducting phase coherence by thermally excited spinon-vortices.

Furthermore, our study investigates the contribution of both a -spinons and b -spinons to the uniform static susceptibility χ^{loc} , as expressed by

$$\chi^{\text{loc}} = \chi_b^{\text{loc}} + \chi_a^{\text{loc}}. \quad (\text{S31})$$

To derive the uniform static susceptibility χ_b^{uni} for b -spinons, we introduce the external magnetic field in Eq. (S9), represented as $-2\mu_B \sum_i S_i^z H$. This inclusion leads to the Zeeman splitting effect in the b -spinon dispersion given by:

$$E_{m,\sigma}^b = E_m^b - \sigma\mu_B H, \quad (\text{S32})$$

where E_m^b is defined in Eq. (S13). Consequently, the total magnetic moment induced by the magnetic field from b -spinons can be expressed as:

$$M_b = \mu_B \sum_m [n_B(E_{m,\uparrow}^b) - n_B(E_{m,\downarrow}^b)] \quad (\text{S33})$$

where $n_B(\omega) = 1/(e^{\beta\omega} - 1)$ denotes the bosonic distribution function. Therefore, the χ_b^{loc} at local site is defined by $\chi_b^{\text{loc}} = \frac{M_b}{NB} |_{H \rightarrow 0}$, resulting in

$$\chi_b^{\text{loc}} = \frac{2\beta\mu_B^2}{N} \sum_m n_B(E_m)[n_B(E_m) + 1], \quad (\text{S34})$$

The temperature evolution of χ_b^{uni} as described in Eq. (S34) is depicted by the black solid line in Fig. S4(c). It can be observed that χ_b^{uni} decreases as the temperature decreases due to the strengthening antiferromagnetic correlations, which oppose the uniform polarization of the spin. Moreover, the existence of an energy gap in b -spinons leads to the opening of a gap at low temperatures, approximately below T_c . The values of the parameters used in our calculations are determined by the mean-field self-consistent equations presented in Ref. 37 and 38.

Furthermore, the uniform static susceptibility χ_a^{loc} for a -spinons can be derived by setting $\mathbf{q} \rightarrow 0$ and $\mu \rightarrow 0$ in Eq. (5), resulting in

$$\chi_a^{\text{uni}} = \frac{2}{N} \sum_{\mathbf{k}} n_F(E_{\mathbf{k}}) [1 - n_F(E_{\mathbf{k}})] \quad (\text{S35})$$

where $n_F(\omega) = 1/(e^{\beta\omega} + 1)$ denotes the fermionic distribution function. At low temperature, χ_a^{loc} in Eq. (S35) can be further simplified as a temperature-independent Pauli susceptibility directly related to the density of states (DOS) $\mathcal{N}(0)$ at the Fermi surface. However, itinerant fermionic a -spinons possess a BCS-type gap Δ_a , leading to

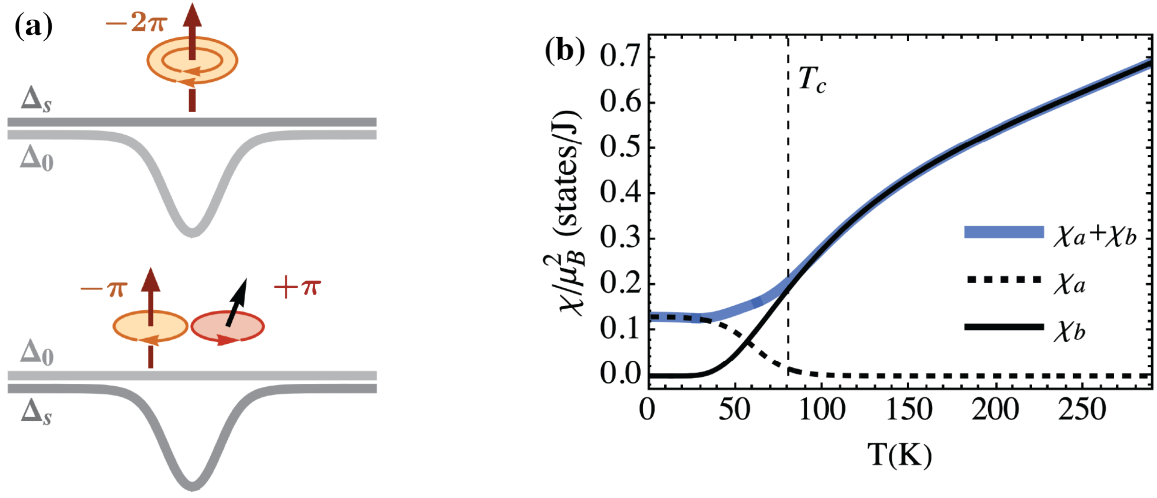


FIG. S4. Illustration for two types of vortices under a magnetic field in (a) and (b). (a) Conventional 2π vortex trapping -2π external magnetic flux [labeled by red arrows], with Δ_a suppressed at the vortex core but Δ_s is preserved. (b) Novel π vortex trapping $-\pi$ external magnetic flux [denoted by the red arrow], along with a free b -spinon [indicated by the black arrow]. In this case, Δ_s is suppressed at the vortex core, while Δ_a is preserved. (c) The temperature evolution of static uniform spin susceptibility, with black solid line denoting χ_b^{loc} in Eq. (S34), with black dashed line denoting χ_a^{loc} in Eq. (S35), with blue line denoting χ^{loc} in Eq. (S31). Notably, the variations in χ^{loc} under the magnetic field are discernible when comparing χ_b^{loc} (black solid line) and χ^{loc} (blue line).

the disappearance of $\mathcal{N}(0)$ and uniform static susceptibility χ_a^{loc} . However, itinerant fermionic a -spinons possess a BCS-type gap Δ_a , resulting in the disappearance of $\mathcal{N}(0)$ and the uniform static susceptibility χ_a^{loc} . Nevertheless, the application of a strong magnetic field can suppress Δ_a at conventional 2π vortex cores, leading to the restoration of a finite DOS with $\mathcal{N}(0) = \frac{a^2}{2\pi\hbar^2} m_a$ contributed by the gapless Fermi pockets of a -spinons. This restoration induces a finite residual χ_a^{loc} given by:

$$\chi_a^{\text{loc}} = 2\mathcal{N}(0) = 2\frac{a^2}{2\pi\hbar^2} m_a F(T) \quad (\text{S36})$$

where an additional coefficient $F(T)$ is introduced to account for the temperature effect of conventional 2π -vortex, which only exists below temperature T_c . The specific expression of $F(T)$ is irrelevant for the structure of χ_a^{loc} , and for simplicity of representation, we assume $F(T) = [\exp[(T - 0.75T_c)/0.1T_c] + 1]^{-1}/4$. Therefore, the black dashed line in Fig. S4(c) represents χ_a^{loc} .

As the result, the total uniform static susceptibility χ^{loc} in Eq. (S31) under a strong magnetic field, is depicted by the blue line in Fig. S4(c). Comparing it with the case without magnetic fields, in which χ_a^{loc} vanishes completely [shown by the black solid line in Fig. S4(c)], we observe the emergence of a finite residual χ^{loc} under a strong magnetic field when $T < T_c$. This finding is consistent with the NMR measurements.

V. Comparison of $\text{Im}\chi^{\text{RPA}}$ in Eq. (7) for Various Parameters

In the main text, we select specific values for the fitting parameters at $\delta = 0.1$, namely $2\Delta_a = 1.1E_g$, $m_a = 1/J$, and $g = 60\text{meV}$, to match the experimental data, where $J = 120\text{meV}$ represents the bare spin exchange interaction. Furthermore, we present the results of $\text{Im}\chi^{\text{RPA}}(q)$ determined by Eq. (7) for different parameter choices at $\delta = 0.1$ in Fig. S5. These results clearly demonstrate that the presence of the hourglass structure is not significantly affected by the specific values of these parameters, as long as the gap $2\Delta_a$ is not too different from the resonance energy $E_g = 2E_s$. This condition is reasonable because the BCS-type pairing Δ_a for a -spinons originates from the RVB pairing Δ_s for b -spinons, following the relation $|\Delta_a|^2 \simeq \delta^2 |\Delta_s|^2$.

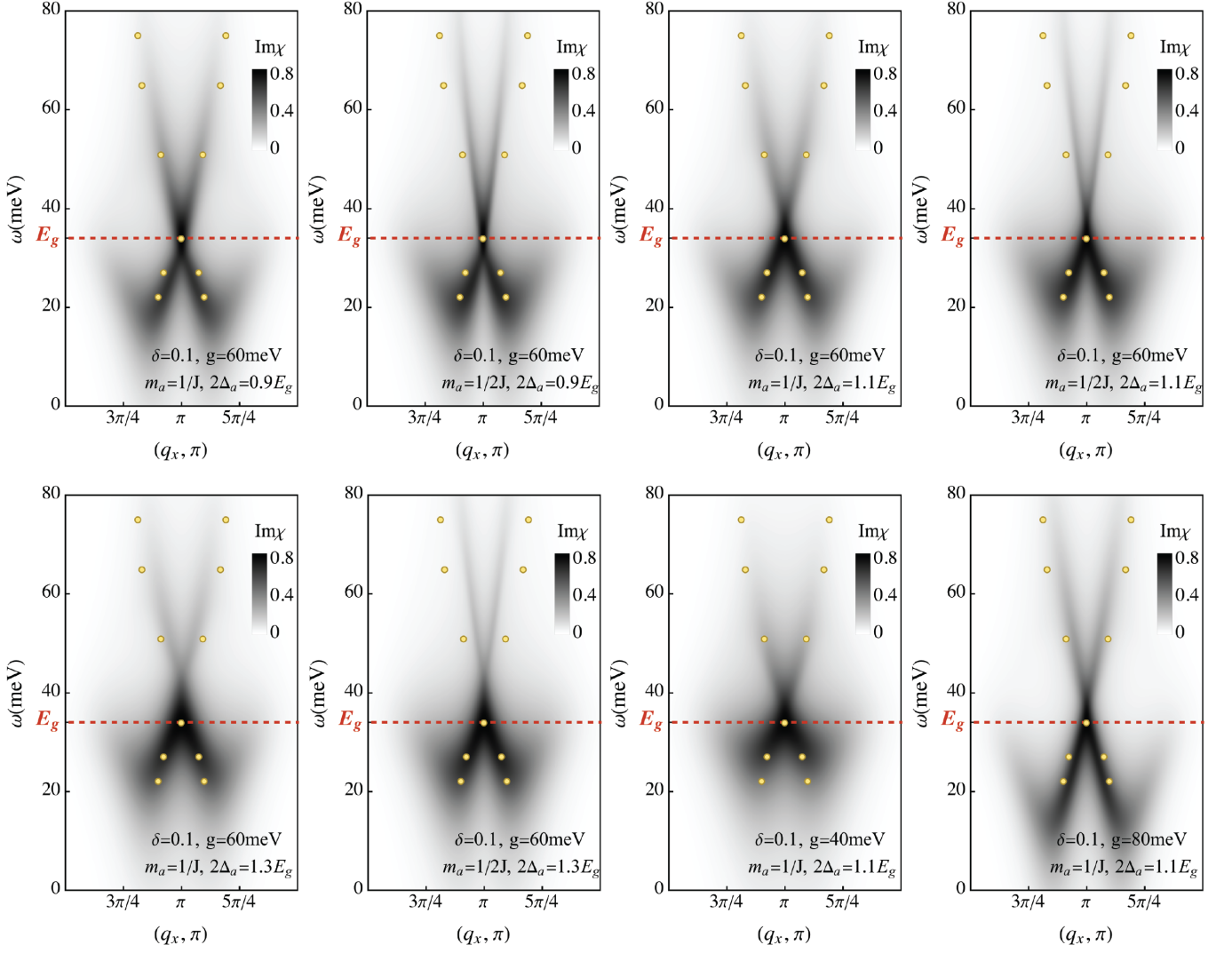


FIG. S5. Imaginary part of dynamic spin susceptibility at RPA level, $\text{Im}\chi^{\text{RPA}}(q)$, determined by Eq. (7) around AFM wave vector \mathbf{Q}_0 at $\delta = 0.1$ with varying parameters.